



A SHORT REVIEW OF MONTE-CARLO HADRONIC CASCADE CALCULATIONS
IN THE MULTI-TEV ENERGY REGION*

N. V. Mokhov
Institute for High Energy Physics, Serpukhov, USSR

and

J. D. Cossairt
Fermi National Accelerator Laboratory, Batavia, IL 60510 USA

September 1985

*Submitted to Nuclear Instruments and Methods A.

1. Introduction

The first superconducting high energy proton accelerator, the Fermilab Tevatron, is now successfully utilized for fixed target physics at a proton energy, E_0 , of 800 GeV. Worldwide there are at least three superconducting proton accelerators being considered for the next generation; the Accelerating Storage Complex (UNK) at Serpukhov, USSR ($E_0 = 3$ TeV), the Large Hadron Collider (LHC) at CERN ($E_0 = 10$ TeV), and the Superconducting Super Collider (SSC) in the USA ($E_0 = 20$ TeV).

The interactions of proton beams of such high energy with matter result in a number of design problems including heating effects due to the intense energy deposition in matter (especially in the superconducting magnets), radioactivation of components, background in experiments, and environmental radiation which may escape the shielding of the accelerator. The most practical method of doing the requisite three dimensional hadronic-electromagnetic cascade calculations is the Monte-Carlo technique. This method has been employed by the authors of the following computer programs; CASIM at Fermilab [1], MARS at IHEP Serpukhov [2,3] and FLUKA at CERN [4]. In the present work selected results using these programs are compared with each other and with existing experimental data. This is done to ascertain the degree of confidence with which the shielding calculations pertinent to the multi-TeV accelerators can be made.

2. Features of the Codes

The three codes studied here simulate the interactions and transport of particles in three-dimensional geometrically complex systems and have many features in common. Detailed descriptions of the physical models used and the codes themselves are given in the primary references [1-4]. Here only highlights of the specific features will be given.

CASIM, when coupled to the program AEGIS [5], simultaneously traces electromagnetic showers induced by decays of neutral pions. The hadron production model of CASIM is a modified version of the Hagedorn-Ranft thermodynamical model. It includes a high transverse momentum correction and some low energy nuclear effects. The maximum incident proton energy, originally restricted to $E_0 \leq 10$ TeV has been recently increased to 50 TeV [6]. The threshold momentum of the hadrons followed is 300 MeV/c. Normally, protons, neutrons, and charged pions are transported. This program uses an inclusive scheme for hadron-nucleus interactions with energy and momentum conservation averaged over a number of collisions. Particles are traced using a step method with fixed step sizes. The particles are transported through an arbitrary geometry defined by the user in a FORTRAN subroutine. Inclusion of magnetic fields in detail is quite simple.

Considerable modifications to CASIM have been made over the years in addition to the AEGIS insertion. Quite satisfactory experimental verifications of this code for a variety of geometry types and sizes and for several different quantities of interest have been made for incident proton energies up to 800 GeV [7-10].

The program MARS has also been improved over the past several years. The most recent version, MARS10, retains the older features along with the following significant improvements. The description of the hadron inclusive spectra (using a selection scheme similar to that of CASIM) relies on the additive quark model of hadron-nucleus interactions [11] for $X_F > 0$ and a phenomenological model [12] for $X_F \leq 0$ (where X_F is Feynman's scaling variable). A set of semi-empirical formulae [3] is used to simulate low energy particle production. Multiple Coulomb scattering is treated using Moliere's theory with allowance for nuclear size effects [13]. An iteration-step method is used in constructing the three-dimensional trajectories for arbitrary geometry in a manner amenable to inclusion of magnetic fields [14]. A modified version of AEGIS [5] is used to handle electromagnetic showers.

The maximum incident energy is extended to 30 TeV, though the program has been used to yield crude estimates up to 10^4 TeV in DUMAND acoustical studies [15]. Protons, neutrons, and charged pions exceeding a threshold energy of 10 MeV may be transported.

At CERN, the program FLUKA82 [4], developed from FLUKA [16] is used. In contrast with the other two programs, FLUKA82 is a full analog simulation of the hadronic cascade. In this program the particle production model used at momenta below 5 GeV/c describes inelastic collisions as quasi-two-body processes producing resonances which subsequently decay. At higher momenta up to about 10 TeV/c a multichain fragmentation representation is employed for particle production. The newest version provides exact quantum number,

momentum, and energy conservation for the extra-nuclear cascade particles. New inelastic cross sections for energies up to 10 TeV are also included. In general cases, participants of cascades considered in the 50 MeV to 10 TeV region are p , \bar{p} , n , \bar{n} , π^+ , π^- , K^+ , K^- , K^0 , \bar{K}^0 , Λ , and $\bar{\Lambda}$. Detailed Monte-Carlo treatment of the electromagnetic showers is presently not included in FLUKA82. The combinatorial geometry package used in this code is a modification of that originally developed at ORNL for the neutron and photon transport program MORSE [17].

3. Selection of Examples of Predictions

In recent years many people have studied macroscopic consequences of high energy proton beam interactions [2, 6, 18-21]. Below, a selection of results using these three programs for the 0.3 to 20 TeV energy region is given. Only hadronic-electromagnetic cascade effects will be presented here, neglecting the very important problem of muons at the new generation of accelerators considered elsewhere [6, 18, 22]. The quantities chosen for comparison are basic ones common to the output of all three codes; the star density $S(\vec{r})$ and the energy deposition density $E(\vec{r})$. The former determines the scale of the biological shielding, the degree of induced radioactivity, and (sometimes) experimental backgrounds. The latter determines the heating and consequent damage to targets, beam dumps, extraction septa, and (perhaps most critically) the superconducting magnets. These quantities are both related to the radiological parameter absorbed

dose, D. The three programs are compared by applying them to cases of solid absorbers which are easy to program or are already available in the literature. Reference to the name of each code refers to the most advanced version of it mentioned above.

Figure 1 shows a comparison of CASIM and MARS10 results with experimental data [7] obtained from the observed temperature increase in segmented targets irradiated by 300 GeV protons. Agreement of both codes with experiment is excellent. In Fig. 2 the radial distributions of energy deposition density in a copper target calculated by all three codes are given for a 400 GeV proton beam incident in a Gaussian spot size having standard deviation $\sigma = 1.25$ mm. The predictions again agree well with experiment [23] but the FLUKA82 and CASIM curves slightly underestimate the measured values.

Figure 3 shows results of a comparison of calculations using CASIM, MARS10, and FLUKA82 [19] for 450 GeV protons incident on a copper cylinder of length 250 cm and radius 20 cm. A beam spot having $\sigma = 1$ mm was used. Agreement is sufficient for most purposes but FLUKA82 predicts smaller values for $S(\vec{r})$ at the larger radii. The total number of stars produced in this cylinder as calculated by CASIM, MARS10, and FLUKA82 are, respectively, 510, 483, and 443 per incident proton and thus are in reasonable agreement.

Table 1 lists values of absorbed dose measured along the outer surface of an iron block of dimensions 91cm by 91cm transverse by 370cm longitudinal, struck by 800 GeV protons as reported in Ref. 10 along with CASIM and MARS10 predictions. In this case the agreement is adequate for most purposes.

For the proton energy region unavailable to existing accelerators, Figs. 4-6 give the calculated star density, $S(r)$, as a function of radius in an iron dump of 500 cm length and 100 cm radius for proton energies of 3, 10, and 20 TeV, respectively. The beam spot is taken to be a Gaussian with $\sigma = 5$ mm. The FLUKA82 calculations shown here were taken from Ref. 20. Both the radial distributions of star density at cascade maxima and the longitudinally integrated values of $S(r)$ are presented. The results are in good agreement with each other.

Figures 7 and 8 show the calculated energy deposition density for this same beam dump bombarded by 10 TeV protons. Included are examples of lateral and longitudinal distributions. CASIM and MARS10 results are consistent, with slightly different longitudinal distributions.

An important quantity for many applications is the maximum energy deposition density. Calculated values of this quantity for cascades initiated by 10 TeV protons incident on large graphite and aluminum blocks are given as a function of the standard deviation of Gaussian beam spots in Fig. 9. FLUKA82 results, taken from Ref. 20, underestimate those of CASIM and MARS10 (which essentially agree) by a factor as large as three. There are two plausible reasons for such a large discrepancy:

1. As pointed out in Ref. 21, only the radial bin $0 \leq r \leq 0.5 \sigma_{\min}$ corresponds to the real maximum energy deposition density in these calculations. In the CASIM and MARS10 runs this bin was specifically studied but in Ref. 20 the inner bin may

have been larger, leading to an "artificial" underestimate.

2. At energies $E_0 \geq 0.5$ TeV the maximum value of energy deposition density is dominated by the electromagnetic showers induced mainly by decays of neutral pions [2]. The semiempirical algorithm used in FLUKA instead of a more precise treatment of electromagnetic showers may be less accurate at these high energies.

As one can see from Figs. 1-9 the results agree very well for different conditions and over a wide energy range. This is gratifying in view of the rather different hadron production and transport schemes used.

4. Moyer Model Parameter

Figure 10 shows the peak absorbed dose calculated along the sides of the iron block studied in Ref. 10 as a function of incident proton energy. Also shown is the total number of stars per proton in the same dump. Calculations have also been made using MARS10 over the range in proton energy from 70 GeV to 20 TeV. The CASIM results from Ref. 10 are also shown in this plot. The value of absorbed dose D presented in Figure 10 is correlated with the parameter of the Moyer shielding model which contains the energy dependence for lateral shielding in a fixed geometry. This semiempirical shielding model has been recently described [24] and revised [25]. In these two references it is shown that the dose equivalent, H , outside of a given geometry is given by,

$$H \propto E^D$$

Since it is not expected that the energy spectrum of the neutrons which dominate the dose equivalent in this situation will change significantly with energy, one can replace dose equivalent H with absorbed dose D in the above relation. The results from Fig. 10 for the peak absorbed dose can, then, be fitted by the following equation:

$$D = aE_0^b \quad (\text{Gy/proton, } E_0 \text{ in GeV}).$$

Applying the results of the calculations to this formula we obtain:

$$\left. \begin{array}{l} \text{CASIM [10]} \quad a = 3.0 \times 10^{-15} \\ \quad \quad \quad b = 0.84 \end{array} \right\} 200 \leq E_0 \leq 800 \text{ GeV}$$

$$\left. \begin{array}{l} \text{MARS10} \quad a = 4.4 \times 10^{-15} \\ \quad \quad \quad b = 0.81 \\ \quad \quad \quad a = 7.8 \times 10^{-15} \\ \quad \quad \quad b = 0.74 \end{array} \right\} \begin{array}{l} 400 \leq E_0 \leq 20000 \text{ GeV (good fit)} \\ 70 \leq E_0 \leq 20000 \text{ GeV (poorer fit)} \end{array}$$

(The poorer fit obviously results from the larger domain in E_0 which was chosen.)

It is also reasonable that the total number of stars per proton in the the iron dump as calculated with MARS10 behaves in the same manner,

$$S = 4.38 E_0^{0.81} \quad 70 \leq E \leq 20000 \text{ GeV.}$$

5. Computational Features

Using a CDC CYBER-875 as a reference computer we have found that MARS10 to be somewhat faster than CASIM. For example, to run 1000 cascades initiated by 10 TeV protons in the large iron beam dump

described in section 3 with the energy deposition calculated using AEGIS, CASIM required 360 seconds of CPU while MARS10 required 163 seconds. Both programs are thus viable options to use for thick shielding problems if one uses a large number of incident protons. CASIM requires approximately 90000 octal words of storage while MARS10 requires about 40000. However the standard version of CASIM allows for five different materials to be used while MARS10 only allows for three. In general, for the same number of incident protons followed, CASIM results are typically smoother than are those of MARS10 for the same spatial bins.

In these considerations, FLUKA82 differs sharply from the other two codes. It needs approximately 400000 words of memory. As mentioned in Ref. 19, to calculate 86 cascades induced by 450 GeV protons in the 25 cm long copper cylinder, FLUKA82 required 600 seconds of CPU on the SIEMENS-7880 computer. The successful solution of the thick shielding problem would be hindered by these considerations. On the other hand, FLUKA82 with its exclusive scheme of particle production allows for analog simulation of hadron cascades which is indispensable in the study of fluctuation problems, in e.g. hadron calorimeters.

6. Conclusion

All three programs considered here are compatible with the calculations needed for the multi-TeV accelerator era. Each has its own features which have advantages for some types of calculations and

disadvantages for others. The predictions of these three programs are in sufficient agreement to allow one to do cascade calculations in this energy region up to 20 TeV with confidence. Nevertheless, the subject of future work should emphasize the updating of the hadron production models to reflect recent experimental and theoretical developments.

We would like to thank A. Van Ginneken for his very helpful comments on this paper.

REFERENCES:

1. A. Van Ginneken, Fermilab Report FN-272, Fermilab, Batavia, IL, USA, 1975.
2. N. V. Mokhov, IHEP Preprint 82-168, Serpukhov, USSR, 1982.
3. A. N. Kalinovsky, N. V. Mokhov, and Yu. P. Nikitin, "Penetration of High Energy Particles Through Matter", Energoatomizdat, Moscow, USSR, 1984.
4. P. A. Aarnio, J. Ranft, and G. R. Stevenson, CERN TIS-RP/106, 1983.
5. A. Van Ginneken, Fermilab Report FN-309, 1978.
6. A. Van Ginneken, in "Report of the 20 TeV Hadron Collider Workshop", Cornell University, March 28-April 2, 1983.
7. M. Awschalom, P. J. Gollon, C. Moore, and A. Van Ginneken, Nucl. Instr. and Meth. 131 (1975) 235.
8. M. Awschalom, S. Baker, C. Moore, A. Van Ginneken, K. Goebel, and J. Ranft, Nucl. Instr. and Meth. 138 (1976) 521.
9. J. D. Cossairt, N. V. Mokhov, and C. T. Murphy, Nucl. Instr. and Meth. 197 (1982) 465.
10. J. D. Cossairt, S. W. Butala, and M. A. Gerardi, Nucl. Instr. and Meth. A238 (1985) 504.
11. J. Nyiri, V. V. Anisovich, Yu. M. Shabelsky, and M. M. Kobrinsky, preprint KFKI-1982-32, Budapest, 1982.
12. E. Stenlund and I. Otterlund, Preprint CERN-EP/82-42, 1982.
13. I. S. Baishev, N. V. Mokhov, and S. I. Striganov, preprint IHEP 84-210, Serpukhov, 1984, to be published in "Yadernaya Physica".
14. M. A. Maslov and N. V. Mokhov, preprint IHEP 85-8, Serpukhov, USSR, 1985.
15. G. A. Ascarian, B. A. Dolgosheln, A. N. Kalinovsky, and N. V. Mokhov, Nucl. Instr. and Meth. 164 (1979) 267.
16. J. Ranft and J.T. Routti, Comput. Phys. Commun. 7 (1974) 327.
17. M. B. Emmett, ORNL Report-4972, 1975.
18. J. D. Cossairt and A. J. Elwyn, Fermilab Report FN-404, 1984.

19. G. R. Stevenson, CERN TIS-RP/IR/84-12, 1984.
20. A. Fasso, K. Goebel, M. Höfert, H. Schonbacher, and G. R. Stevenson, CERN TIS/RP/IR/84-20, 1984.
21. N. V. Moknov, Fermilab Report, FN-328, 1980.
22. M. A. Maslov, N. V. Moknov, and A. V. Uzunian, Nucl. Instr. and Meth. 217 (1983) 419.
23. P. Sievers, CERN TM-SPS/ABT/77-1, 1977.
24. G. R. Stevenson, Lin Kuei-Lin, and R. H. Thomas, Health Phys. 43 (1982) 13.
25. R. H. Thomas and S. V. Thomas, Health Phys. 46 (1984) 954.

TABLE 1

Absorbed Dose (GY/incident proton X 10^{-13})

Longitudinal Coordinate (cm)	35	60	195	205
---------------------------------	----	----	-----	-----

Experiment (Ref. 10)	5.1 \pm 0.5	6.7 \pm 0.5	3.5 \pm 0.4	3.5 \pm 0.4
-------------------------	---------------	---------------	---------------	---------------

CASIM	3.8 \pm 0.5	6.1 \pm 0.6	3.5 \pm 0.4	2.8 \pm 0.3
-------	---------------	---------------	---------------	---------------

MARS10	5.3 \pm 0.8	7.1 \pm 1.1	2.7 \pm 0.5	2.0 \pm 0.5
--------	---------------	---------------	---------------	---------------

Experimental errors are based on reproducibility while calculational errors are one standard deviation statistics.

LIST OF FIGURE CAPTIONS

1. Energy deposition density measured and calculated in copper and tungsten targets in the geometry of Ref. 7. The targets were a set of segmented cylinders 2.54 cm in diameter. The incident proton energy was 300 GeV.
2. Lateral distributions of energy deposition density at a depth of 45 cm in a copper target irradiated by 400 GeV protons. Also included are comparisons of the three predictions with experimental data from Ref. 23.
3. Radial distributions of the longitudinally integrated star density in copper induced by 450 GeV protons as calculated by the three programs. Histograms denote the MARS10 results while, * is used for the FLULA82, and ■ is used for the CASIM results.
4. Lateral distributions of star density in an iron beam dump longitudinally integrated (stars/cm²) and values at cascade maximum (stars/cm³) for $E_0 = 3$ TeV. Calculations using CASIM are indicated by ■, while histograms are used for MARS10.
5. The same as Fig. 4 but for $E_0 = 10$ TeV. * and 0 denote FLUKA82 results.
6. The same as Fig. 4 but for $E_0 = 20$ TeV.
7. Lateral distributions of energy deposition density in an iron beam dump longitudinally integrated (GeV/cm²) and values at energy deposition density maximum (GeV/cm³) for $E_0 = 10$ TeV. Histograms denote the MARS10 results while the circles denote the CASIM results.
8. Laterally integrated energy deposition distributions and energy deposition densities on the longitudinal axis of an iron dump as a function of depth (Z), the longitudinal coordinate, for $E_0 = 10$ TeV. The same notation as in Fig. 7 is used.
9. Maximum energy deposition densities in aluminum and graphite beam dumps irradiated by 10 TeV protons as a function of the standard deviation, σ , of the beam. Calculational results are denoted: 0, x-FLUKA82 (24), 0, Δ-MARS10, and ■-CASIM
10. Peak absorbed dose and total stars produced as a function of incident proton energy in an iron beam dump 91 x 91 x 370 cm (10). The calculations are denoted: ●-MARS10, 0-CASIM, X-MARS10 (integral). Two different least squares fits to the MARS10 calculations are also included as the dashed and solid curves (please consult the text).

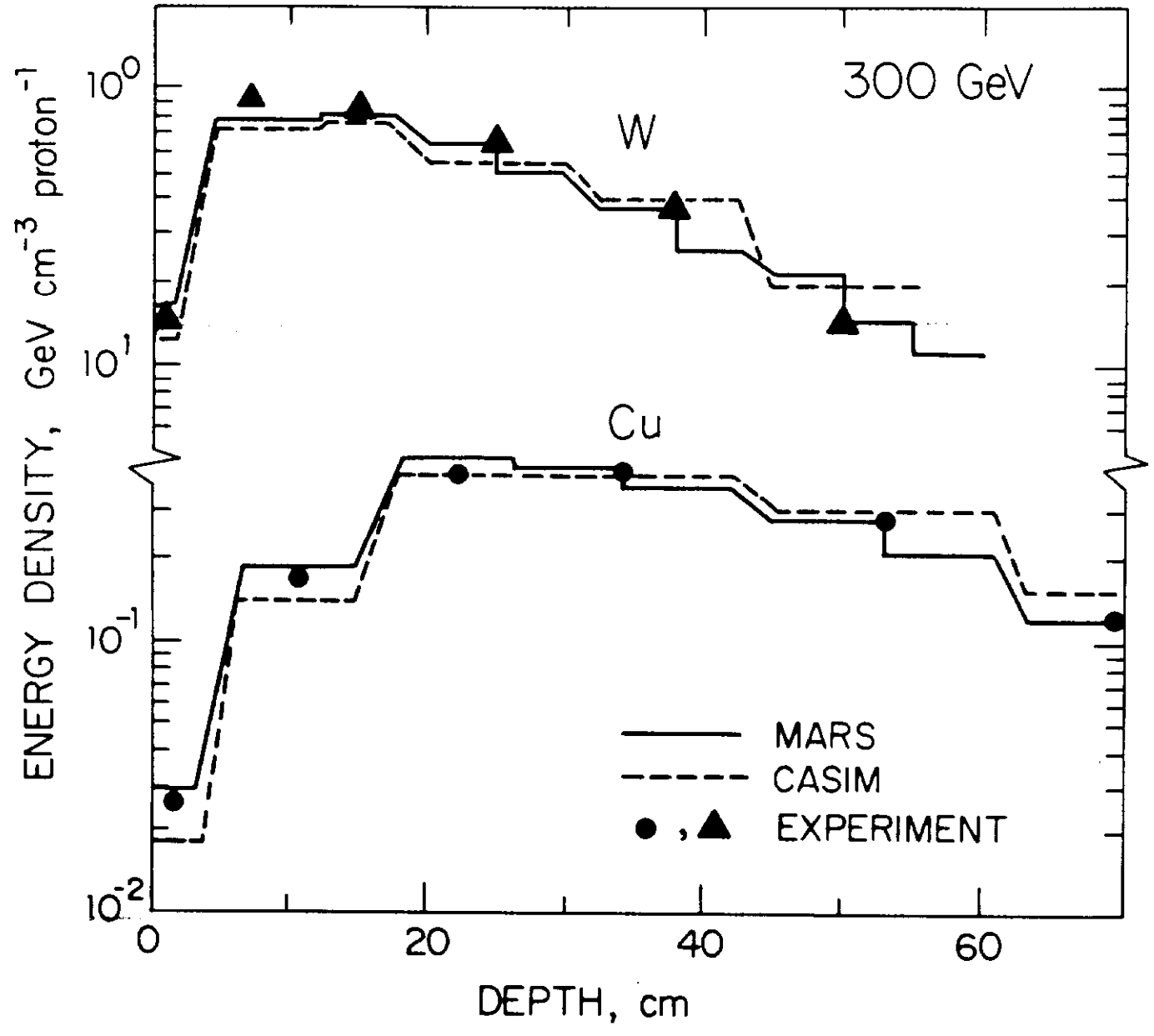


Figure 1

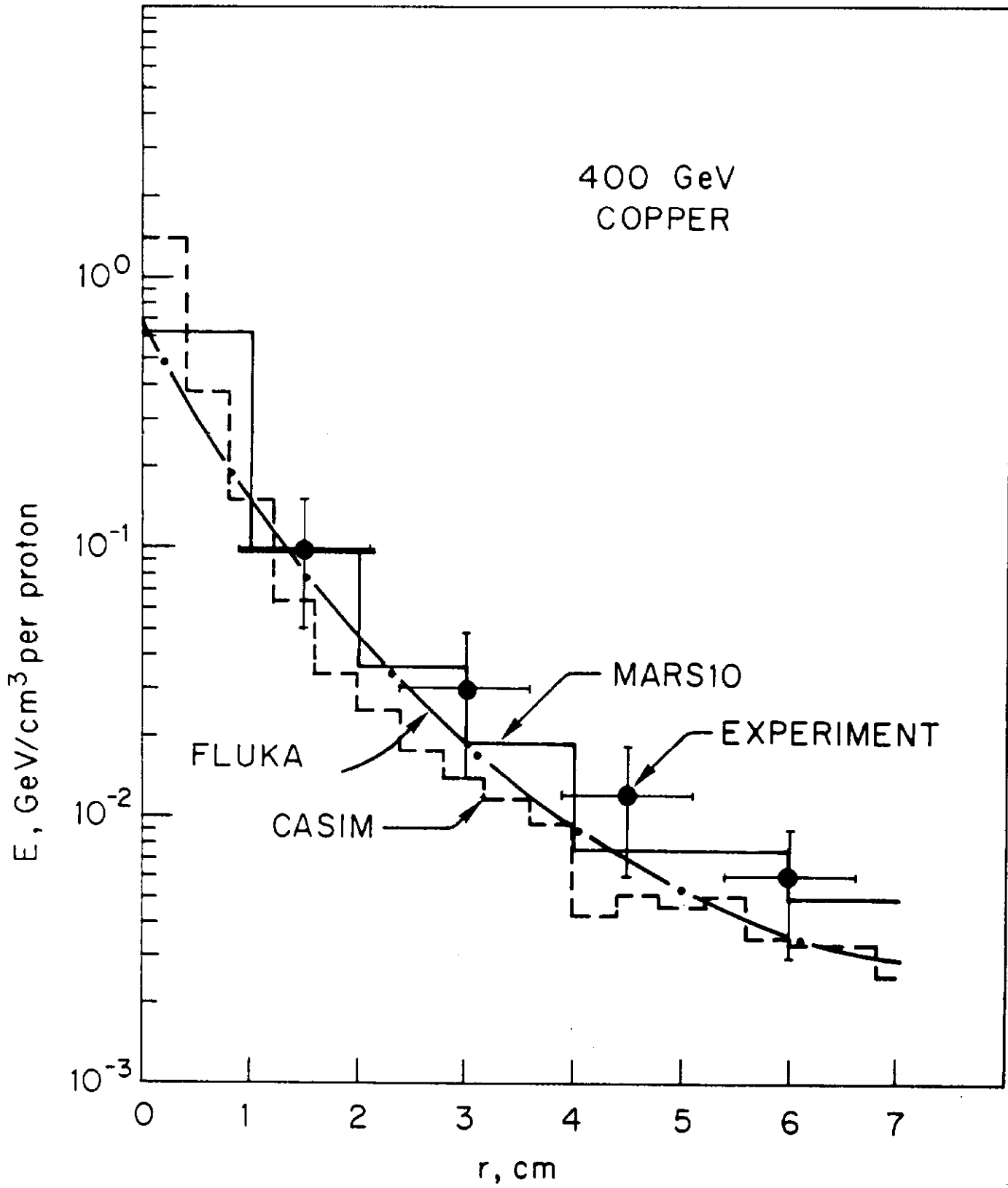


Figure 2

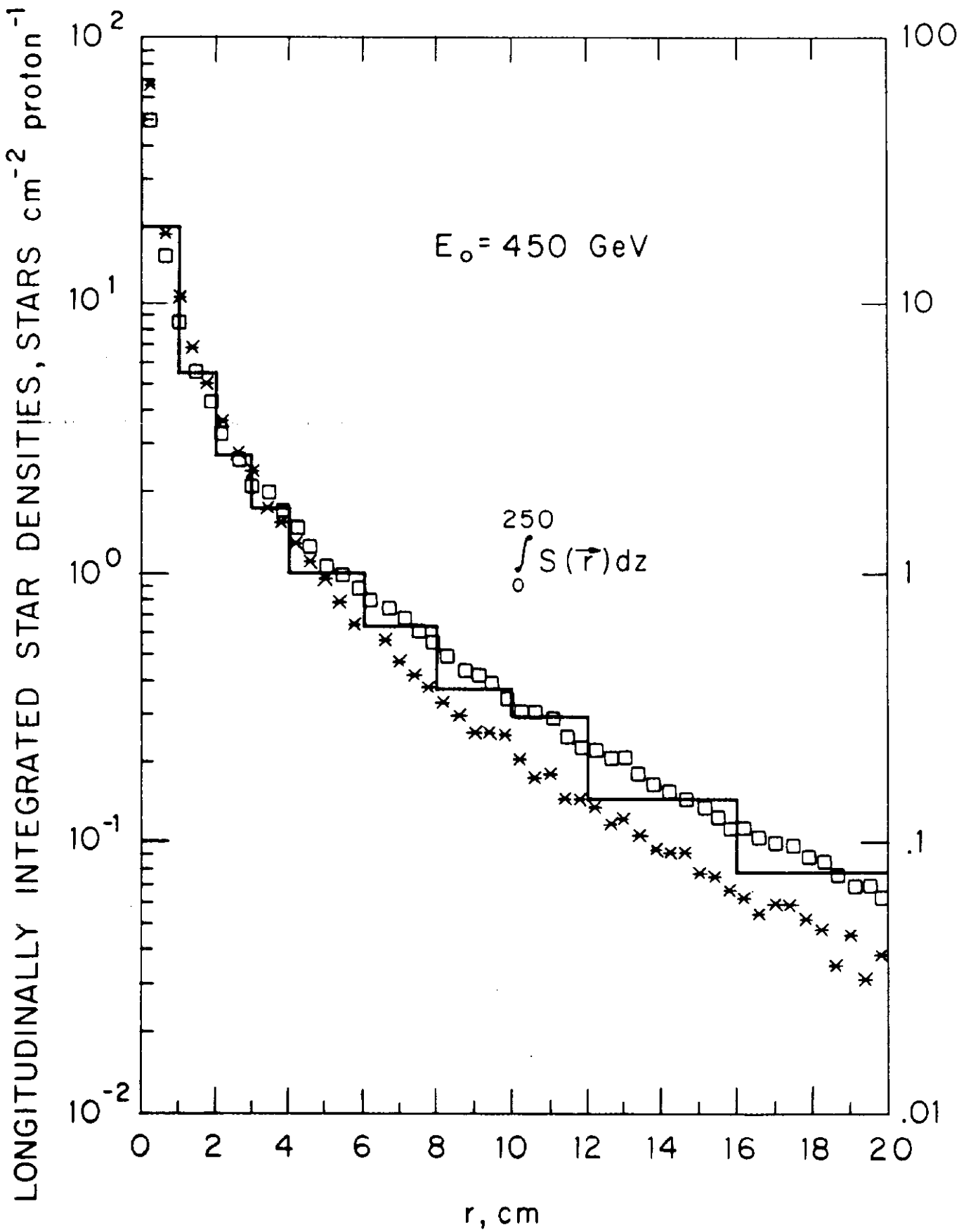


Figure 3

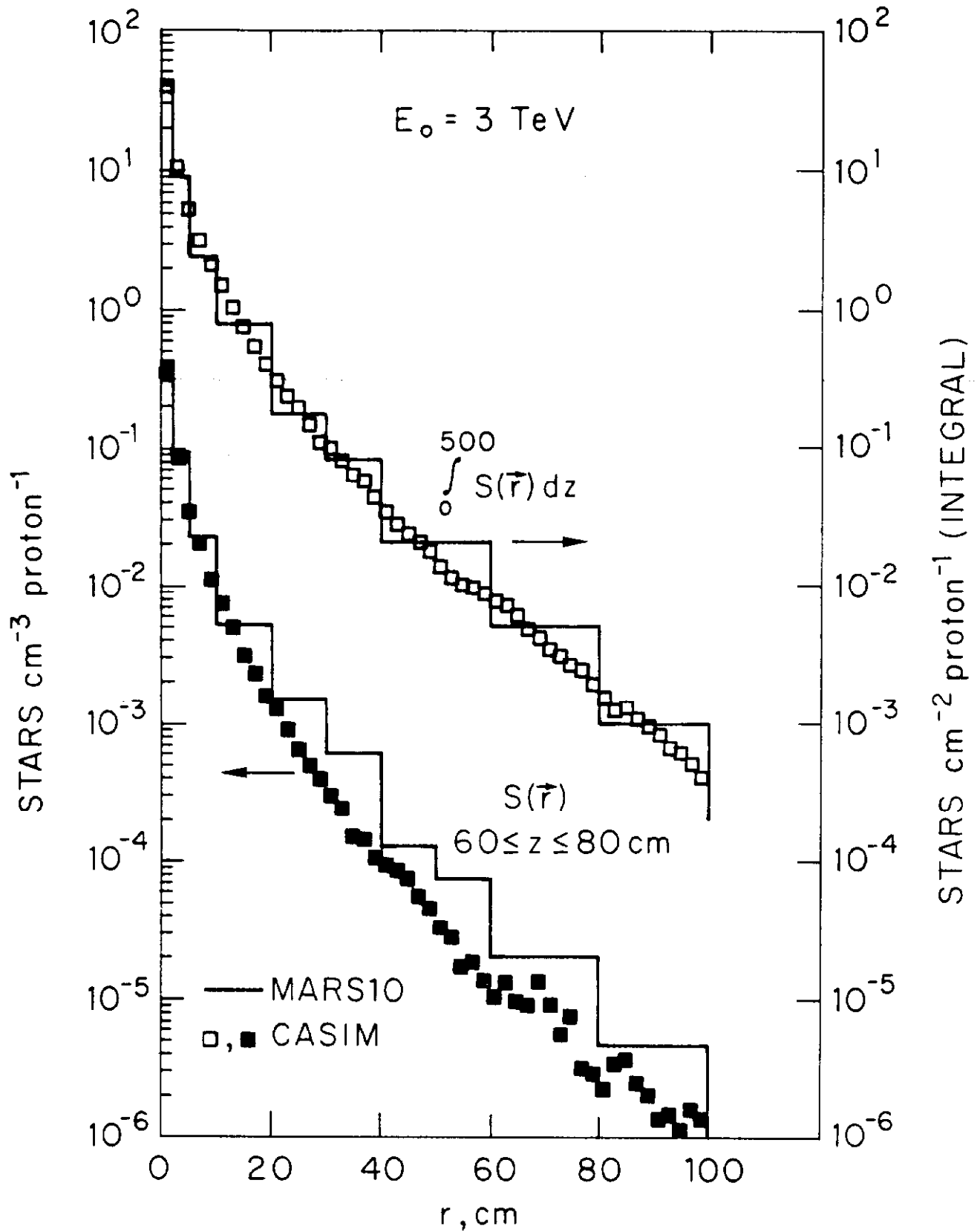


Figure 4

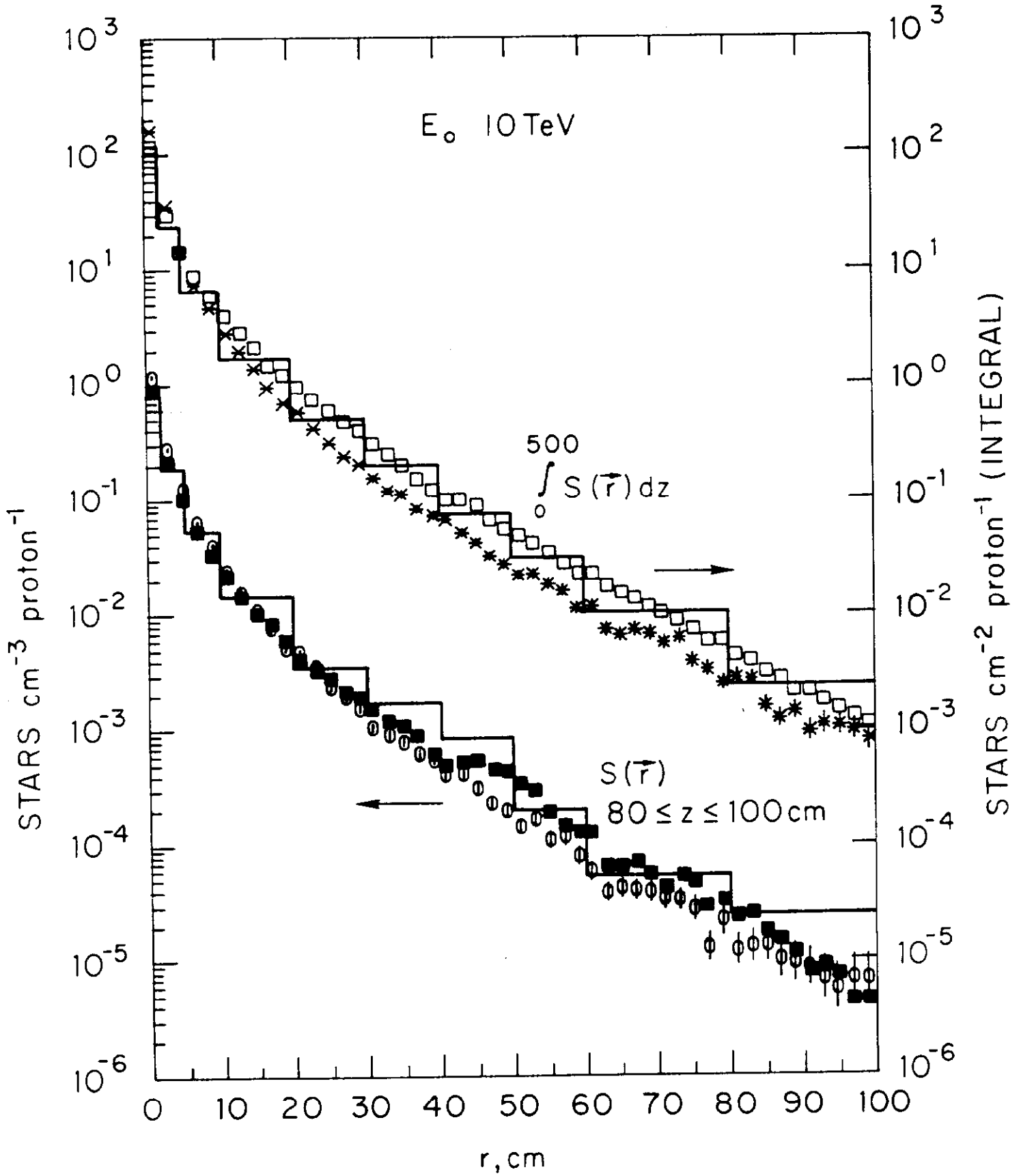


Figure 5

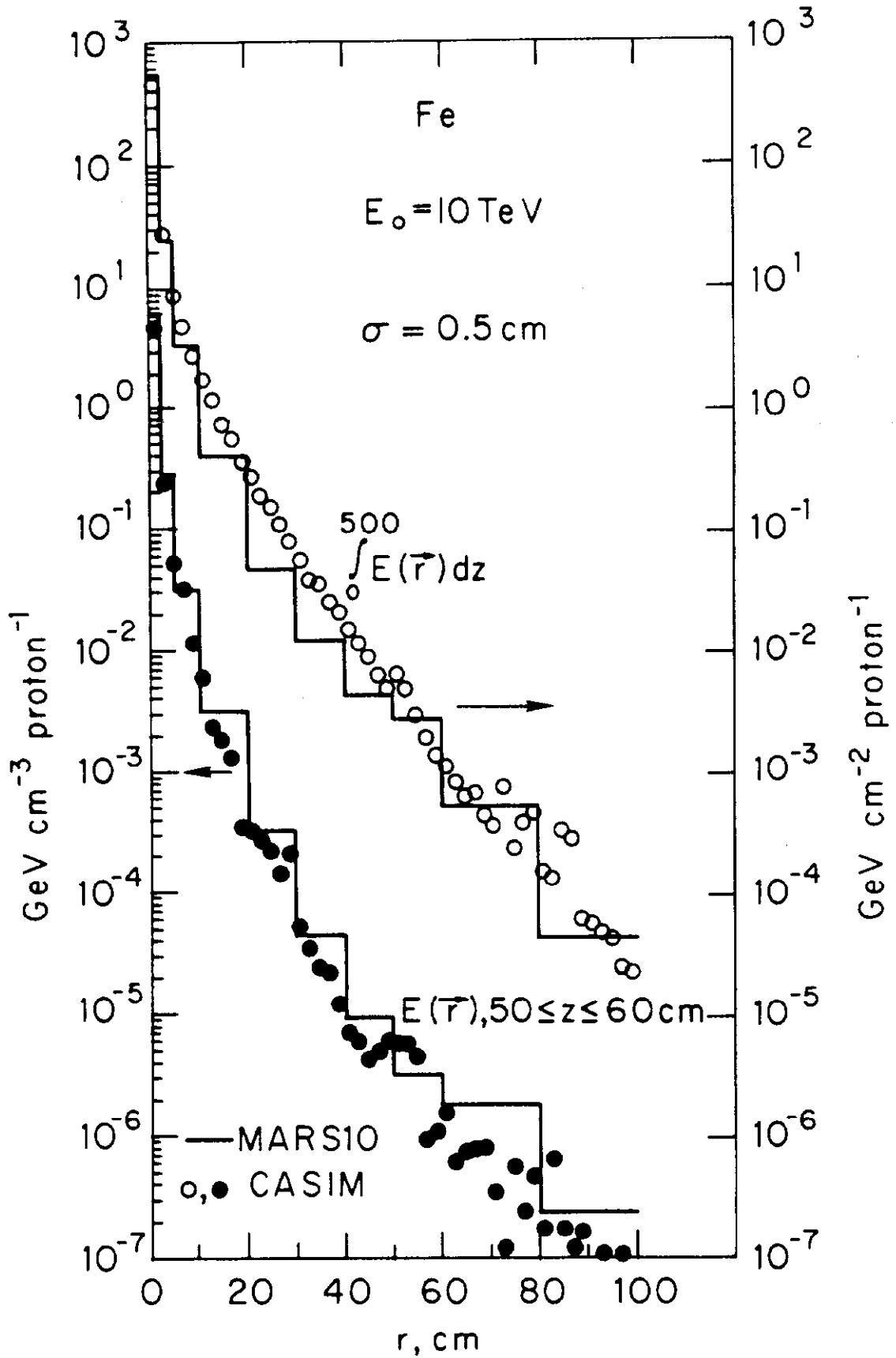


Figure 7

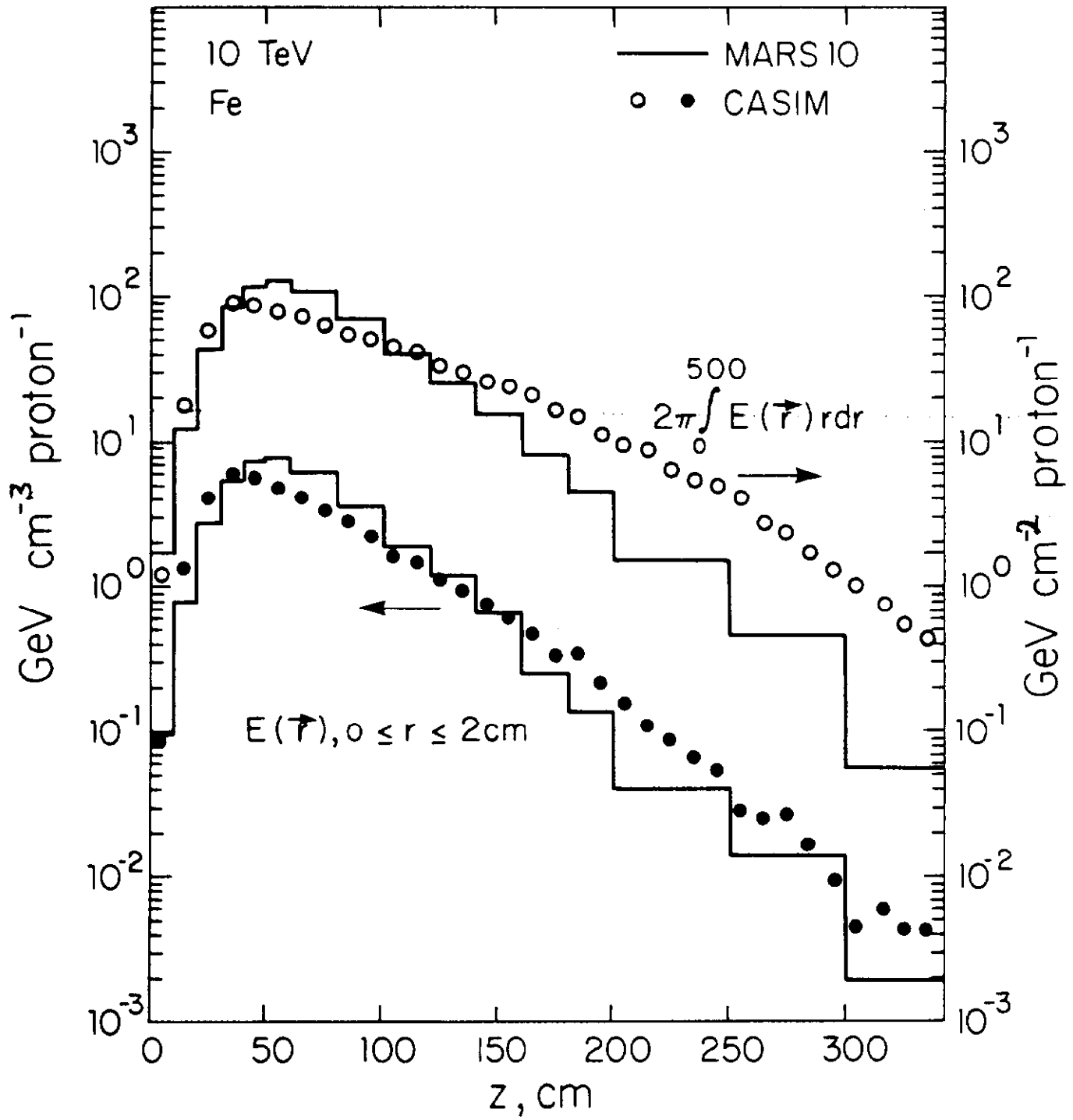


Figure 8

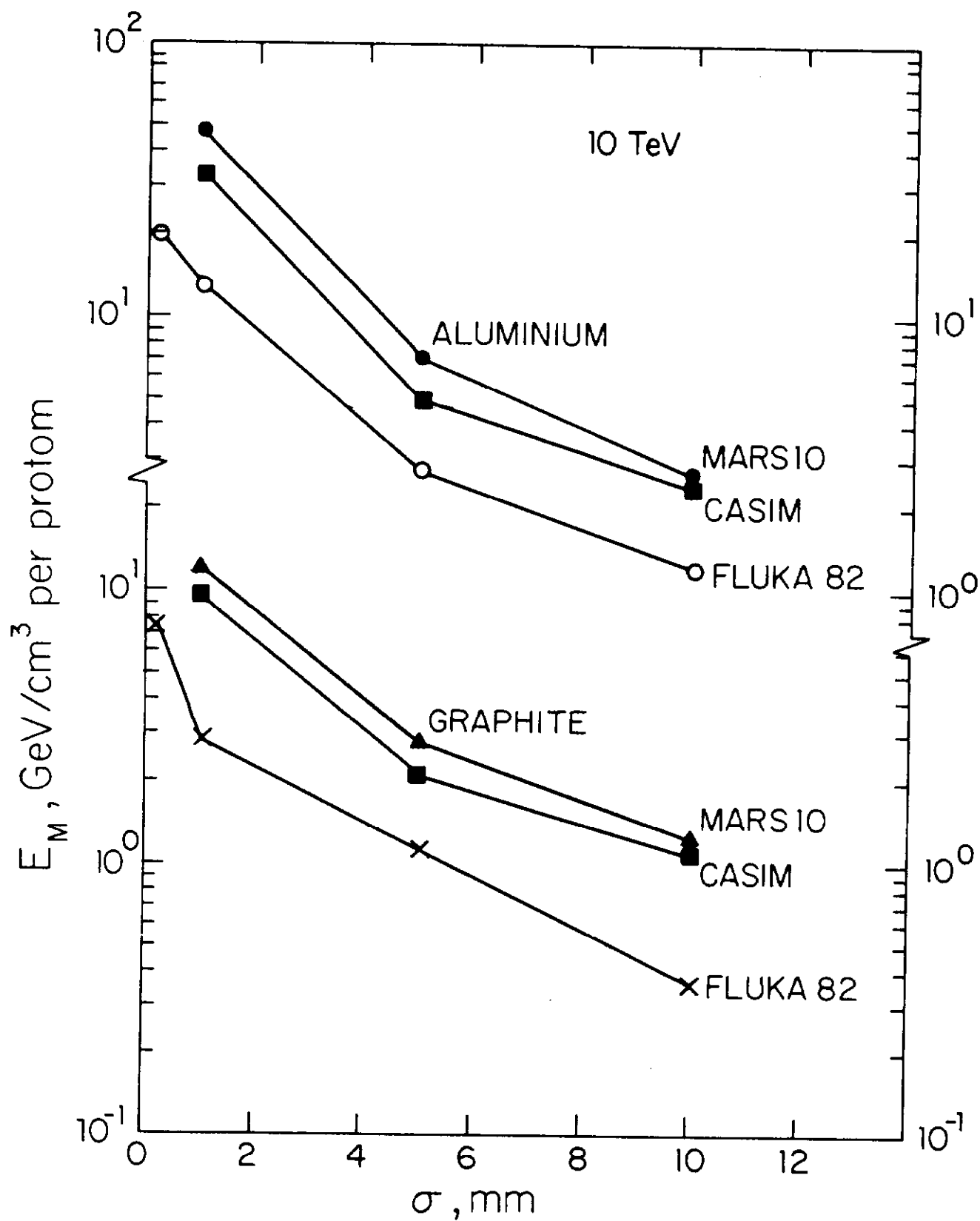


Figure 9

